

NASA Contractor Report 3242

NAS
CR
3242
c.1

LOAN COPY: RETURN TO
AFWL TECHNICAL LIBRARY
KIRTLAND AFB, N. M.

0062097

Infrared Measurements of a Scramjet Exhaust

R. A. Reed and M. W. Slack

CONTRACT NAS1-15395
JANUARY 1980

NASA



0062097

NASA Contractor Report 3242

Infrared Measurements of a Scramjet Exhaust

R. A. Reed and M. W. Slack
Grumman Aerospace Corporation
Bethpage, New York

Prepared for
Langley Research Center
under Contract NAS1-15395



National Aeronautics
and Space Administration

**Scientific and Technical
Information Office**

1980

TABLE OF CONTENTS

	<u>Page</u>
Summary	1
Introduction	2
List of Symbols	3
Experimental Procedure	4
Data Analysis	11
Discussion	16
Conclusions	18
Appendix: Procedure for Updating Results	19
References	22

LIST OF ILLUSTRATIONS

<u>Figure</u>	<u>Page</u>
1 Test Configuration	5
2 Interferometer Spectrometer Field of View	5
3 Scramjet IR Spectra	7
4 Theoretical H ₂ O Spectrum	9
5 IR Emission Time History	10

LIST OF TABLES

<u>No.</u>		
1	Uniformity of Exhaust Gas IR Emission	9
2	Exhaust Gas Parameters Derived from the Infrared Band Ratio Technique	15
3	Exhaust Gas Parameters Derived from Band Integrated Intensity and Theoretical T vs P Law	15
4	Sensitivity Analysis of the Infrared Band Ratio and Band Integrated Intensity Techniques to Inhomogeneous Temperature Distributions	17

SUMMARY

Infrared spectra of the $2.7\text{ }\mu\text{m}$ H_2O ν_3 band were measured from the exhaust gases of the NASA Langley scramjet using a rapid scan interferometer spectrometer. Mass averaged station radiation measurements were made at four different fuel equivalence ratios in order to determine engine combustion efficiencies, and collimated beam measurements were made to confirm the absence of large scale spatial variations in exhaust gas temperature. Except for the lowest (0.2) fuel equivalence ratio, signal levels were adequate for reliable background subtraction and analysis. The arc heater injected negligible noise into the spectrometer system, and no major interference was encountered from thermal continuum emission or from contaminants in the flow. Comparison of mass averaged and collimated beam measurements and the detailed IR emission time history of each test run indicate that combustion in the scramjet engine is nonsteady.

In order to deduce exhaust gas temperature and water vapor partial pressure, two alternative analysis techniques were applied to the data. The first technique, based upon band integrated radiant intensity, requires external specification of a pressure-temperature relation to eliminate one of these two independent variables. The results obtained using this technique are the most reliable indicators of exhaust gas conditions, exhibiting moderate-to-low sensitivities to errors in measurement, errors in the predicted T vs $P_{\text{H}_2\text{O}}$ relation, plume divergence, or inhomogeneous temperature distributions in the exhaust gas. Combustion efficiencies were derived using these results and the known engine operating conditions. Efficiencies ranged from 70–50 percent as the fuel equivalence ratio changed from 0.4 to 1.0. The second technique, based upon the infrared band ratio technique, is superior in principle because it provides independent estimates of water vapor partial pressure and temperature. In practice, however, the propagation of errors due to rather small temperature inhomogeneities in the exhaust gases leads to significant errors in derived temperature — particularly in water vapor pressure $P_{\text{H}_2\text{O}}$ — making this approach strictly applicable only to isothermal sources.

INTRODUCTION

The NASA Langley scramjet is an experimental engine designed to study and verify certain advanced hypersonic propulsion concepts (Refs. 1 and 2). The current prototype is installed in a four-foot-diameter test tunnel and burns hydrogen fuel in a hypersonic air stream for short (5–10 seconds) test intervals. Measurements of exhaust gas temperature and water partial pressure are needed to determine the combustion efficiency of this engine. Since in situ measurement of these quantities is difficult, we have investigated the applicability of nonintrusive remote sensing infrared diagnostics to the scramjet facility. Our specific approach is to monitor the infrared emission of water vapor in the $2.7\text{ }\mu\text{m}$ ν_3 band. The spectral profile and absolute radiant intensity of this band are functions of water vapor temperature and partial pressure, and techniques exist that are capable of deducing these quantities from spectral data. A rapid scan interferometer spectrometer (Ref. 3) was used to measure the scramjet spectra. The broad ($2\text{--}5\text{ }\mu\text{m}$) wavelength coverage of this instrument is important because it provides a means of distinguishing between true water vapor emission and that due to possible flow contaminants (NO_x , Cu, etc.) or thermal background. The excellent time-averaging capabilities of this particular type of instrument are similarly advantageous in the presence of signal fluctuations.

This report describes the IR emission measurements, presents reduced IR spectral data, documents the data analysis, and presents derived combustion efficiencies.

LIST OF SYMBOLS

P_{H_2O}	water vapor partial pressure
P_{static}	static pressure
T	temperature
m	mass fraction at high temperature
$B(\lambda, T)$	Planck radiation function, $W/cm^2-sr-\mu m$
λ	wavelength, μm
f	area filling factor
$I(\lambda)$	radiant intensity, $W/cm^2-sr-\mu m$
r	response function of instrument
l_0	path length along line of sight
ϕ_i	injected fuel equivalence ratio
ϕ_c	combusted fuel equivalence ratio
η	combustion efficiency
R	infrared band ratio
h	Planck's constant
ν	frequency
K_b	Boltzmann constant

EXPERIMENTAL PROCEDURE

Diagnostic 2–5 μm infrared spectra of the NASA Langley scramjet exhaust gases were measured with a rapid scan interferometer spectrometer (Ref. 3) at approximately 30 cm^{-1} ($0.02\text{ }\mu\text{m}$) resolution. System wavelength response was limited by the $2\text{ }\mu\text{m}$ cut-on of a germanium field lens and by the $5.4\text{ }\mu\text{m}$ cut-off of the Indium-Antimonide detector. Exhaust gases were viewed through a sapphire window along a line of sight perpendicular to the engine thrust line and 6 cm downstream of the exit plane (Fig. 1). To obtain mass averaged station radiation measurements, a cylindrical $f/2$ lens was used to produce a slit shaped field of view 3.5 cm wide by 30 cm high (full width at half maximum (Fig. 2)). In situ measurements with a point source IR black-body indicated an overall 10 percent uniformity in response over the 24 cm span of the exit plane. The 25 cm atmospheric path length between the interferometer and the sapphire window was left unpurged since atmospheric water vapor absorption over this small range is negligible. To check on the spatial uniformity of the exhaust gases, the field of view was reduced to a 2.5 cm diameter circle. This permitted spatially resolved measurements of spectra from the central, upper, and lower portions of the exit plane.

The interferometer was operated remotely from the engine control room. Raw signals (interferograms) were recorded continuously on analog FM tape over the full duration of each run to check for background emission level shifts, and to study the detailed time behavior of the infrared emission. The arc heater injected negligible noise into the system, but introduction of the warm air flow into the tunnel produced a noticeable (20 percent) rise in the thermal emission background level. As a precautionary measure, the portion of the test chamber wall directly opposite the sapphire viewing window was painted flat black to minimize the possibility of diffuse reflectance of intense hot engine parts radiation into the field of view. The net ratio of signal to background depended upon fuel equivalence ratio, but was typically 10:1, so that background subtraction was not difficult. The start of fuel injection for each run was recorded by a signal ganged to the fuel valve solenoid. IR data collected during brief transient starting periods ($\sim 1\text{ sec}$) were disregarded.

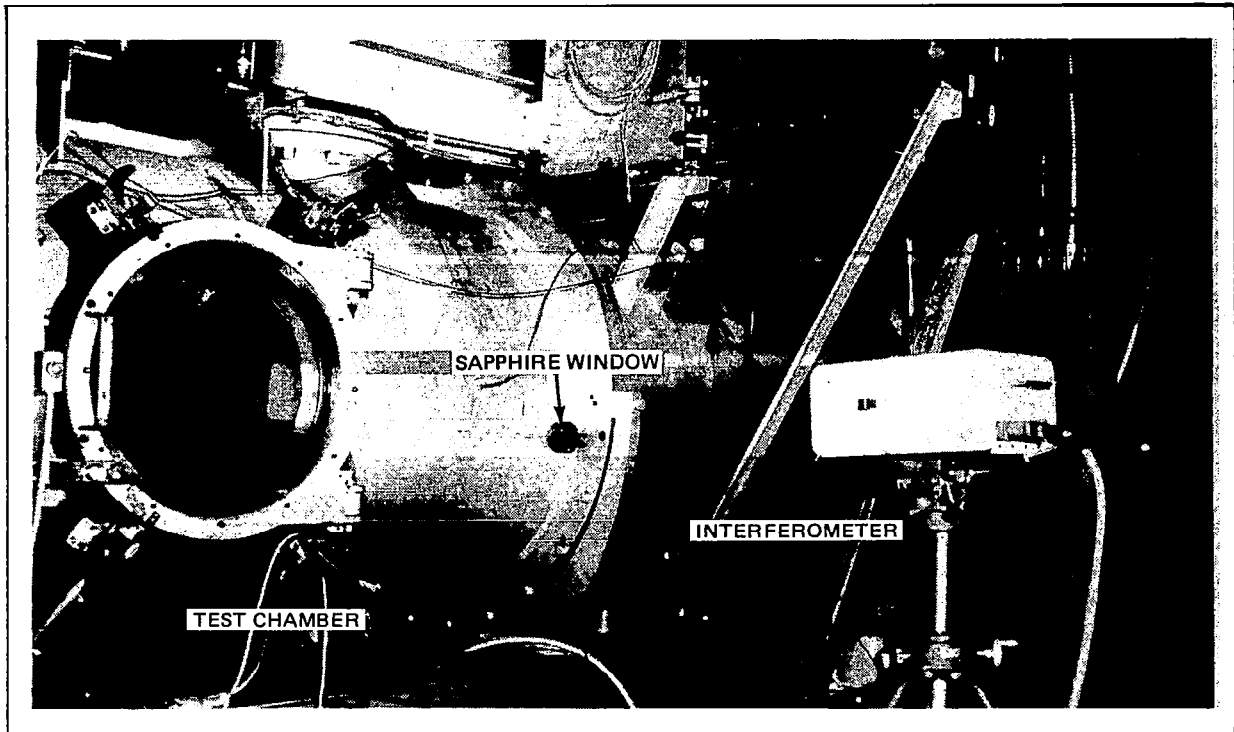


Fig. 1 Test Configuration. Scramjet IR emission was received through a sapphire window mounted on the test chamber wall and monitored with an interferometer spectrometer

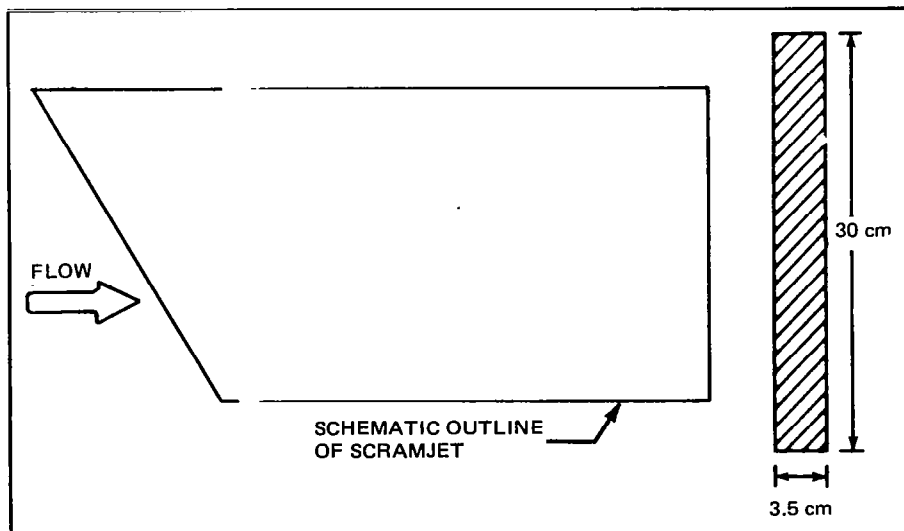


Fig. 2 Interferometer Spectrometer Field of View. Primary field of view was an elongated rectangle situated 6 cm aft of the scramjet exit plane. Field of view was reduced to a 2.5 cm diameter circle for selected test runs

System calibration was performed using a wide aperture IR blackbody reference source, the same optics and sapphire window, and the identical distances employed in the scramjet measurement. Calibrated spectral radiance was corrected for background emission and filling factor according to the formulae

$$I(\lambda) = \frac{V^* - V^*(BG)}{V(BB) - V(BG)} \times \frac{B(\lambda, T)}{f} \quad (1)$$

$$f = \int_{-L/2}^{L/2} r(z)dz \div \int_{-\infty}^{\infty} r(z)dz \quad (2)$$

where

V^* = scramjet exhaust raw signal

$V^*(BG)$ = scramjet background raw signal

$V(BB)$ = blackbody reference source raw signal

$V(BG)$ = blackbody background raw signal

$B(\lambda, T)$ = Planck function

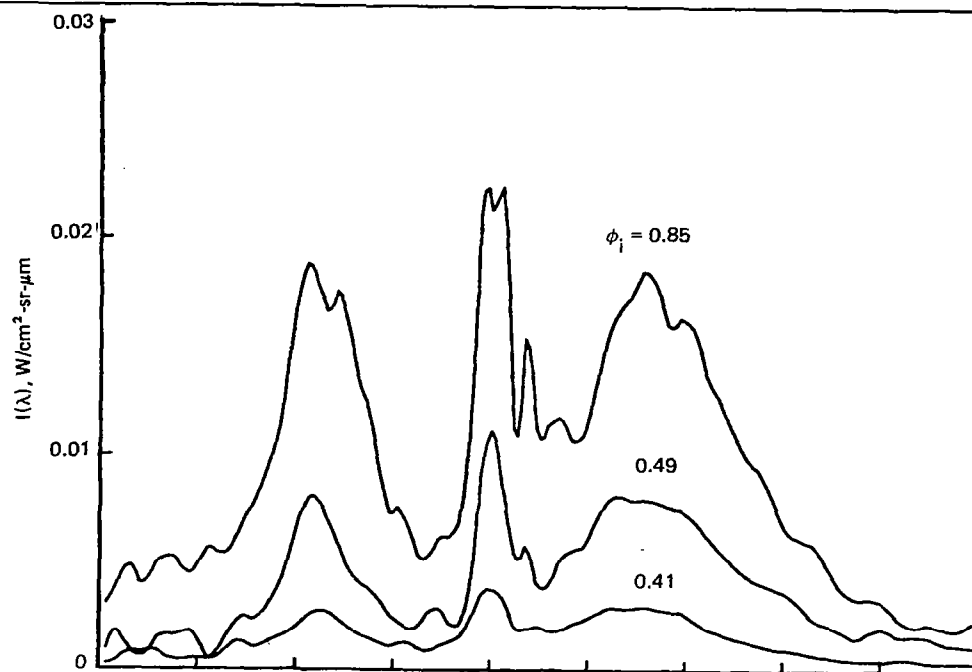
f = field of view filling factor

L = vertical height of scramjet exit plane

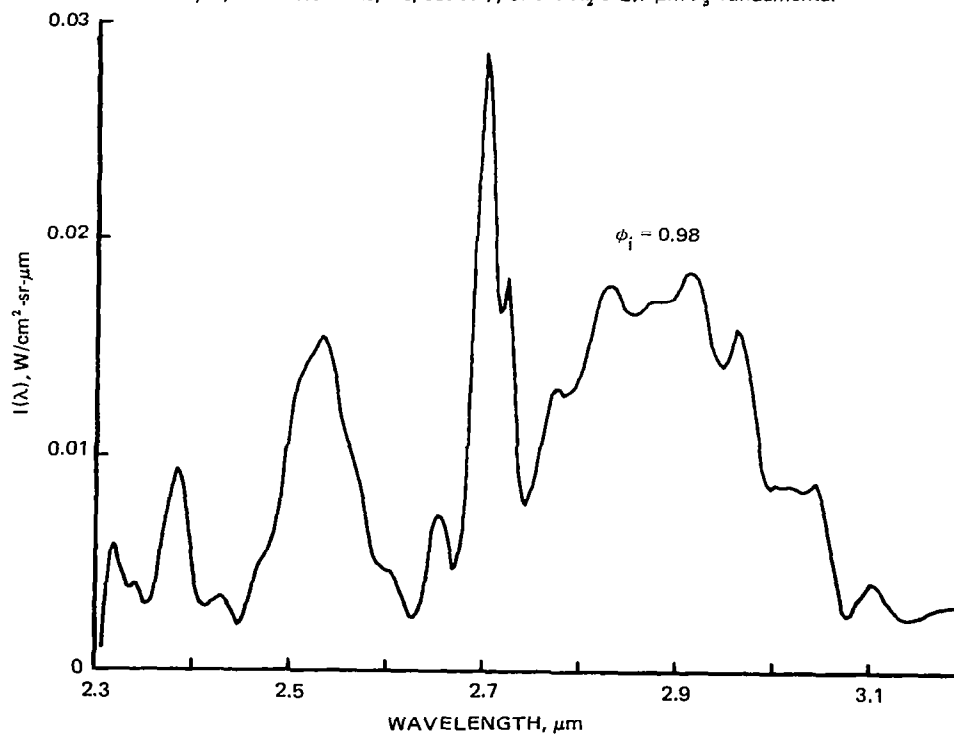
$r(z)$ = instrument vertical response function across field of view

The filling factor accounts for the size difference between the scramjet exit plane and the blackbody reference source.

The observed mass averaged spectra are shown for various fuel equivalence ratios in Fig. 3. These spectra exhibit the characteristic P, Q, and R branch structure of the ν_3 H_2O band with peaks near 2.9, 2.7, and 2.5 μm , respectively, and their intensity rises monotonically with increasing fuel equivalence ratio ϕ_1 . The infrared intensity at low ϕ_1 value (0.2, not shown) is too low for reliable background correction. The spectrum for the highest ϕ_1 value, 0.98, represents the transform of a single scan of the interferometer and consequently is relatively noisy; the limitation to a single scan was due to engine unstart and test run termination. The remaining spectra are time averaged (2–4 seconds) results with fair scan-to-scan repeatability. The spectra show no evidence for interfering emission from hot metal parts, nitric oxides, or the



A. Measured exhaust H_2O vapor IR spectra showing monotonic increase with fuel equivalence ratio ϕ . Intensity maxima near 2.5, 2.7, and 2.9 μm correspond to the R, Q, and P-branches, respectively, of the H_2O 2.7 μm ν_3 fundamental



B. Spectrum measured for highest fuel equivalence ratio $\phi = 0.98$. (Noise due to engine unstart and abrupt test run termination)

Fig. 3 Scramjet IR Spectra

zirconium oxide overcoating used on certain scramjet components. Figure 4 shows that the scramjet spectral profiles agree with the expected shape of the $2.7\text{ }\mu\text{m}$ water band based upon Grumman radiation code calculations (Ref. 5). This particular theoretical spectrum corresponds to a temperature of 1400K and an H_2O pressure-path-length product of 168 N/m, roughly that expected for a fuel equivalence ratio of 1 and a combustion efficiency of 50 percent (cf. Fig. 3b).

A characteristic of the scramjet infrared radiance is its fluctuating intensity level. For each run, appreciable signal fluctuations began abruptly at the point of fuel ignition, producing a noisy interferogram signal similar to those of turbulent jets and flames (Ref. 4). These fluctuations were considerably less for mass averaged data ($3.5\text{ cm} \times 24\text{ cm}$) than for spatially resolved data (2.5 cm diameter). Figure 5 shows how successive scans, taken approximately 0.3 second apart, compare for these two fields of view. Measurements performed with the smaller field of view exhibit considerably greater scan-to-scan fluctuations than those performed with the large field of view. These observations indicate that homogeneous uniform combustion, although useful as an analytic approximation, is an oversimplification of actual conditions within the scramjet combustor.

The purpose of the collimated beam measurements (2.5 cm diameter field of view) was to check for any large scale top-to-bottom variations in IR signal that would be undetected in the mass averaged measurements. Three measurements at a nominal fuel equivalence ratio of 0.5 were made 6 cm downstream at vertical positions 5 cm below the upper lip of the exit plane, on centerline, and 5 cm above the lower lip. Because of the long 1.2 m unpurged path length used for these measurements, only relative signal strengths could be determined. The observed IR emission was fairly uniform, and most of the deviations in raw signal level were attributable to differences in test conditions. After correction for differences in vignetting (± 12 percent) due to the varying look angle through the lens mount and collar, IR radiances were constant to within 15 percent (Table 1). Since radiance varies as roughly the fourth power of temperature or of water vapor partial pressure, uniformity of these plume parameters appears to be substantially better than 15 percent.

TABLE 1 UNIFORMITY OF EXHAUST GAS IR EMISSION

Run	IR Radiance ^a	Approx Temp -H ₂ O Variation ^b
168 (top)	1.05	1.01
167 (center)	1.00	1.00
169 (bottom)	1.14	1.04

^aNormalized and corrected for run-to-run differences in vignetting.
^bNormalized; derived from radiance data.

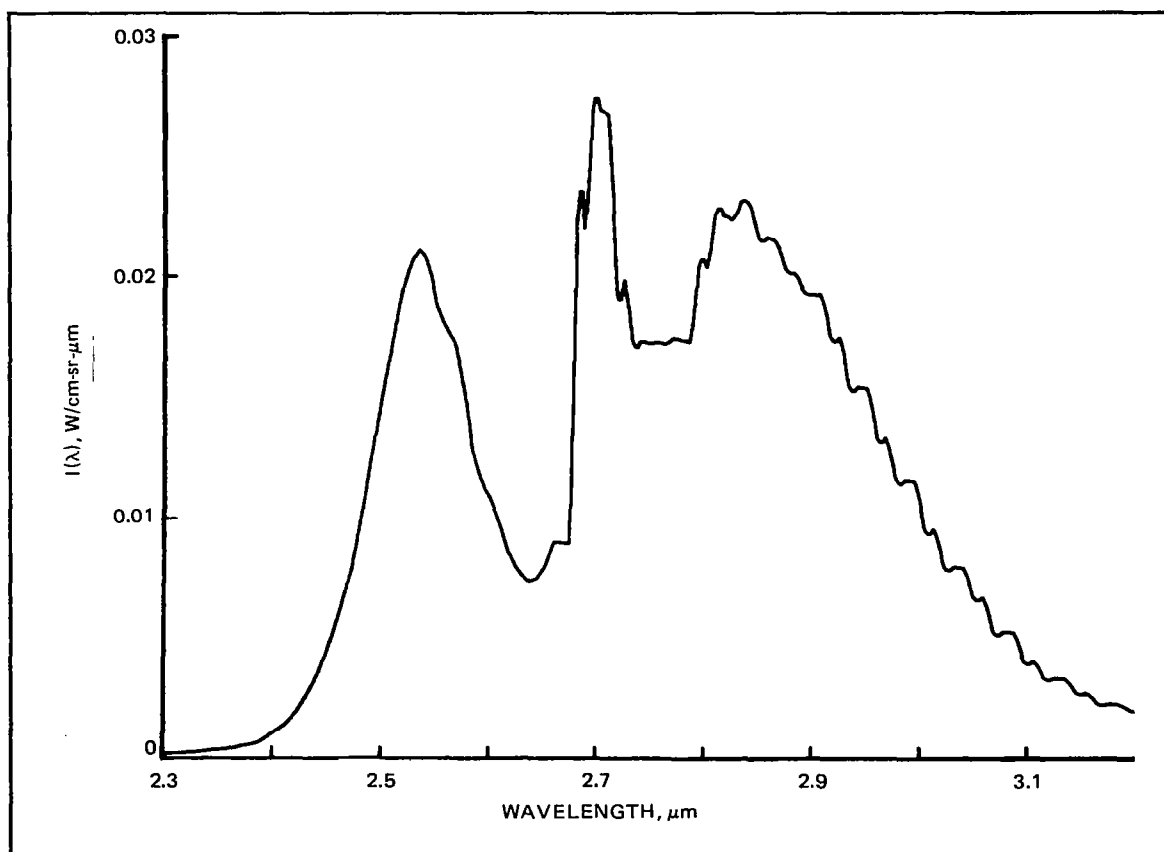


Fig. 4 Theoretical H₂O Spectrum. Predicted radiance for 168 N/m H₂O at 1400K illustrates characteristic spectral profile for comparison with data

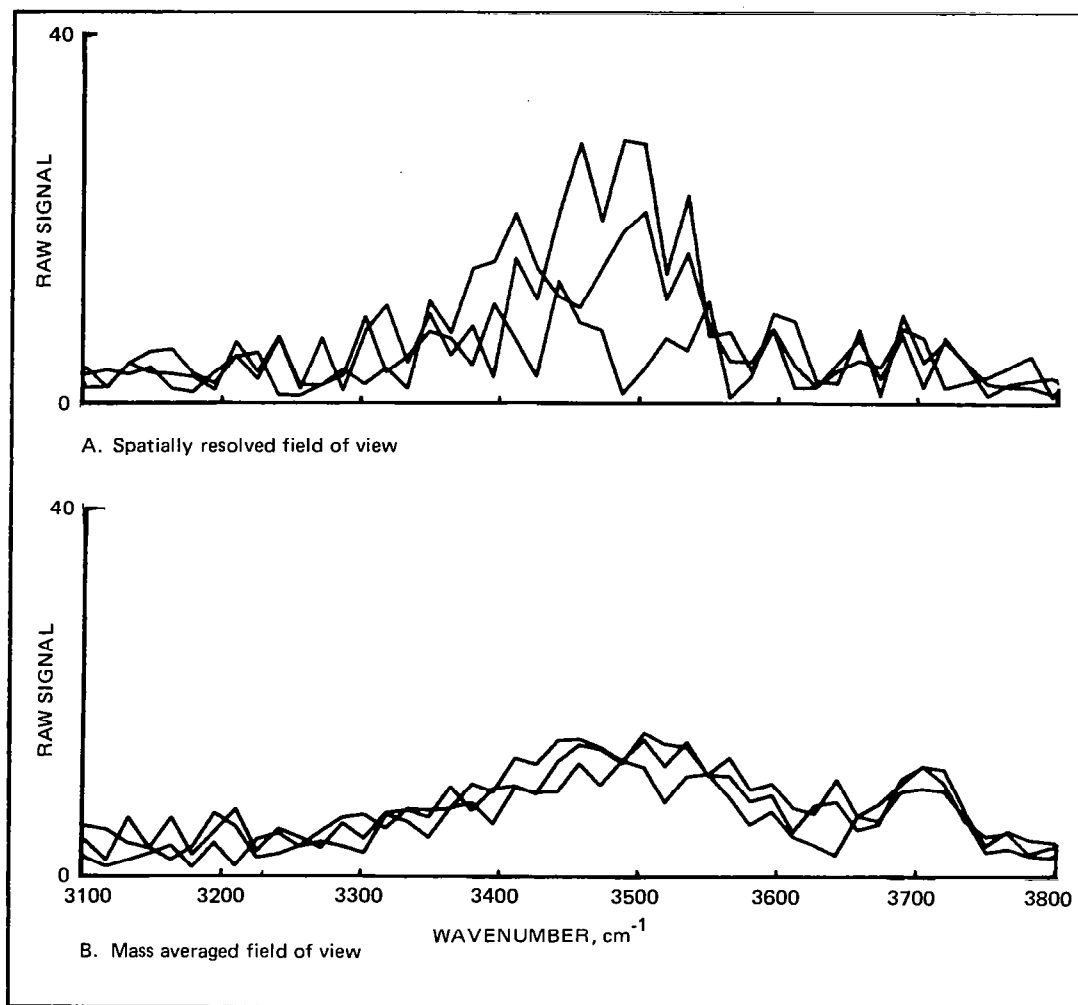


Fig. 5 IR Emission Time History. Successive scans measured approximately 0.3 sec apart using spatially resolved (2.5 cm diameter) and mass-averaged (3.5 cm x 30 cm) fields of view consistently showed different degrees of repeatability, indicative of localized fluctuations in exhaust gas properties

DATA ANALYSIS

The scramjet IR spectra provide two fundamental types of spectroscopic information: absolute radiant intensity and relative spectral shape. Since these two parameters are functions of gas pressure and temperature, a two parameter pressure-temperature fit to the spectral data is possible. For purposes of analysis, two in-band radiant intensities may be defined as

$$\bar{I}_{12} = \int_{2.65}^{2.85} I(\lambda) d\lambda \quad (3)$$

$$\bar{I}_{23} = \int_{2.85}^{3.1} I(\lambda) d\lambda \quad (4)$$

where $I(\lambda)$ is the observed spectral data. The sum

$$\bar{I} = \bar{I}_{12} + \bar{I}_{23} = \bar{I}(P_{H_2O}, T) \quad (5)$$

then serves to describe the absolute intensity level, and the ratio

$$R = \bar{I}_{23} / (\bar{I}_{12} + \bar{I}_{23}) = R(T) \quad (6)$$

then serves to describe the spectral shape. It will be shown that, for the optically thin gas regime pertinent to the scramjet, Eq. (6) provides a convenient measure of temperature that may be substituted into Eq. (5), which prescribes a more complex functional relationship between temperature and water vapor partial pressure. The construction of the parameters \bar{I} and R and the choice of wavelength intervals λ_1 in Eqs. (3) and (4) is based upon fundamental gaseous emission laws and upon the infrared band ratio technique.

The spectral radiance of water vapor is given by

$$I(\lambda) = \epsilon(\lambda, T) B(\lambda, T) \quad (7)$$

where $\epsilon(\lambda, T)$ is the spectral emissivity and $B(\lambda, T)$ is the Planck function. For conditions appropriate to the NASA Langley scramjet, moreover, the exhaust gas is optically thin and emissivity may be set equal to

$$\epsilon(\lambda, T) = k(\lambda, T) P_{H_2O} l_0 \quad (8)$$

where $k(\lambda, T)$ is the molecular emission coefficient, P_{H_2O} the partial pressure of water, and l_0 the path length. Integration of Eq. (7) over the wavelength interval 2.65–3.1 μm specifies a functional P_{H_2O} – T relation implicit in the parameter \bar{I} .

$$\bar{I} = B(\bar{\lambda}, T) \int_{2.65}^{3.1} \epsilon(\lambda, T) d\lambda \quad (9)$$

$$\bar{I} \sim \text{const.} \times B(\bar{\lambda}, T) P_{H_2O} l_0 \quad (10)$$

where $\bar{\lambda}$ specifies a band-weighted wavelength mean and where the fact that $\epsilon(\lambda, T)$ varies much more rapidly than $B(\lambda, T)$ is used to perform the integral. The specific wavelength interval used for \bar{I} has the advantage that $\int \epsilon(\lambda, T) d\lambda$ is only slowly varying with temperature, conveniently placing nearly all the temperature sensitivity in the factor $B(\lambda, T)$.*

The subdivision of the 2.65–3.1 μm wavelength interval into two segments is made to facilitate spectral analysis of temperature using the infrared band ratio technique (Ref. 7). This technique is analogous to two-color optical pyrometry and is based upon the observation that the intensities of certain molecular emission bands are temperature sensitive. In the specific case of the 2.7 μm H_2O band, it is the long wavelength P-branch emission that is most sensitive to temperature, which leads to the specific choice of numerator in the ratio R of Eq. (6). Based upon the H_2O band model data of Young (Ref. 6) and Grumman Plume Code calculations (Ref. 5), this ratio is predicted to be a nearly linear function of temperature over the scramjet operating envelope approximated by

$$T = 1500K + 1720K (R - 0.533) \quad (11)$$

Temperatures derived in this manner agree with a cruder estimate based upon overall spectral width of the H_2O band, as determined from the separation $\Delta\nu_{PR}$ of the P and R branch maxima measured in cm^{-1} (Ref. 8).

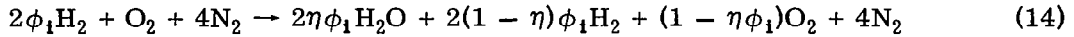
$$T = \Delta\nu_{PR}^2 / 130 \text{ cm}^{-2}\text{K}^{-1} \quad (12)$$

* $\int \epsilon(\lambda, T) d\lambda$ varies $\pm 1.3\%$ between 1000–1500K (Ref. 6)

The water vapor pressure-path length product $P_{H_2O}l_0$ is determined by substitution of Eq. (11) into Eq. (9), and if plume divergence is small, the value of l_0 6 cm downstream can be taken as the exit plane width, $l_0 = 16.2$ cm, giving P_{H_2O} . Combustion efficiencies η are derived from the water vapor partial pressure using the relation

$$\eta = \frac{P_{H_2O}/P_{static} (5 + 2\phi_1)}{(P_{H_2O}/P_{static} + 2)\phi_1} \quad (13)$$

which is derived from the reaction equation



where ϕ_1 is the fuel equivalence ratio. Combustion efficiency is the only parameter affected by errors in fuel equivalence ratio ϕ_1 or in static pressure (determined by engine wall pressures measured near the exit plane). From Eq. (13), efficiency is approximately inversely proportional to the product $\phi_1 P_{static}$

$$\eta \sim \text{const}(\phi_1 P_{static})^{-1} \quad (15)$$

so that the product in Eq. (15) must be well known for reliable efficiency estimates.

The net results of this infrared band ratio analysis are shown in Table 2. Water vapor pressures derived by this method are sensitive to errors in the temperature estimates, as can be seen from Eq. (10).

$$P_{H_2O} = \frac{\text{const} \times \bar{I}}{l_0 B(\bar{\lambda}, T)} \sim \frac{\text{const} \times \bar{I}}{l_0 T^3} \quad (16)$$

A 10 percent overestimate in T results in a 40 percent underestimate in P_{H_2O} (and in combustion efficiency η as well). Thus it can be seen that the error propagation properties of the infrared band ratio technique are unfavorable and require high accuracy in T evaluation for merely moderate accuracy in P_{H_2O} and η .

The results of the infrared band ratio technique are at variance with preliminary theoretical temperature vs water vapor partial pressure predictions for the scramjet exhaust. Theoretical T vs P_{H_2O} predictions can be used in conjunction with the observed absolute radiant intensities, Eq. (5), to eliminate one of the two independent variables T and P_{H_2O} . This procedure has the disadvantage of introducing the inherent uncertainties

of the T vs P_{H_2O} relation into the analysis, but the practical advantage of leading to a much more robust analysis with well behaved error propagation. If temperature is eliminated by substitution of a relationship

$$T = T_{\text{theory}}(P_{H_2O}) \quad (17)$$

then Eq. (5) gives a one parameter fit to the experimental data.

$$\bar{I} = \bar{I}(P_{H_2O}) \quad (18)$$

One particular form of Eq. (17) predicts a nearly linear relation between T_{theory} and the variable ϕ_c , defined as

$$\phi_c = \eta \phi_1 \quad (19)$$

In terms of water vapor mole fraction x , ϕ_c is

$$\phi_c = \frac{x(5 + 2\phi_1)}{x + 2} \quad (20)$$

and this expression can be used to write $T(\phi_c)$ as $T(P_{H_2O})$. For $T(\phi_c)$, in K, given by

$$T = 400 + 2000 \phi_c(1 - \phi_c/10) \quad (21)$$

(G. Anderson, private communication), the derived temperatures, water vapor partial pressures, and combustion efficiencies are shown in Table 3. The sensitivities of P_{H_2O} and T to experimental and theoretical errors is lower for this analysis technique, compensating for the fact that P_{H_2O} and T are no longer determined independently. To first order, both P_{H_2O} and T are linear in the variable ϕ_c , from which we derive

$$\bar{I} \approx \text{const } \phi_c B(\bar{\lambda}, T(\phi_c)) \approx \text{const } \phi_c^4 \quad (22)$$

Thus, for a 15 percent error in \bar{I} , ϕ_c , and thus pressure and temperature, are specified to better than 4 percent. If the T vs ϕ_c law is in error by a fraction $\Delta T/T$ then

$$\bar{I} \text{ (apparent)} \sim \text{const} \left(1 + \frac{\Delta T}{T}\right)^3 \phi_c^4 \quad (23)$$

from which the relative ϕ_c , P_{H_2O} , and T errors are all found to be

$$\frac{\Delta \phi_c}{\phi_c} = \frac{\Delta T}{T} = \frac{\Delta P_{H_2O}}{P_{H_2O}} = \frac{3}{4} \frac{\Delta T}{T} \quad (24)$$

Thus, a 15 percent error in the theoretical T vs P_{H_2O} law results in an approximate 11 percent error in P_{H_2O} and T. In any case, the propagation of errors in this alternative technique is much improved compared to that of the infrared band ratio technique, and unless gross errors (> 25 percent) in the theoretical T vs P_{H_2O} law are suspected, it is the more reliable technique of the two.

TABLE 2 EXHAUST GAS PARAMETERS DERIVED FROM THE INFRARED BAND RATIO TECHNIQUE

Test Parameters			Measured Parameters		
Run	ϕ_i	$P_{static}, N/m^2$	$P_{H_2O}, N/m^2$	T, K	$\eta, \%$
165	0.41	8340	114	1500	10
164	0.49	8390	262	1600	19
166	0.85	7900	566	1625	27
164	0.98	8980	635	1625	24

TABLE 3 EXHAUST GAS PARAMETERS DERIVED FROM BAND INTEGRATED INTENSITY AND THEORETICAL T VS P LAW

Test Parameters			Measured Parameters		
Run	ϕ_i	$P_{static}, N/m^2$	$P_{H_2O}, N/m^2$	T, K	$\eta, \%$
165	0.41	8340	853	950	70
164	0.49	8390	1106	1110	76
166	0.85	7900	1219	1315	56
164	0.98	8980	1342	1320	49

DISCUSSION

Since both the infrared band ratio technique and the band integrated intensity technique are predicated upon a homogeneous isothermal source, it is important to ascertain their validity under more general conditions where spatial or temporal variations in temperature occur.

Sensitivity estimates for the band ratio technique and the band integrated intensity technique can be derived by applying the fundamental analysis equations to synthetic spectral data. As a worst case, a "hot spot" temperature of 2000K can be taken, corresponding roughly to a maximum temperature for H_2-O_2 combustion. This results in maximum distortion of both the band profile and the absolute intensity of IR emission. Synthetic radiances for this case were computed according to

$$I(\lambda) = (1 - m)k(\lambda, T_1) + mk(\lambda, T_2) \quad (25)$$

where m is the mass fraction of the gas occupied by hot spots at temperature T_2 . T_1 is a lower temperature near the mass averaged temperature T_0 determined by energy conservation.

$$mT_2 + (1 - m)T_1 = T_0 \quad (26)$$

$$C_p \sim \text{constant (heat capacity)}$$

Table 4 compares how increasing mass fraction m affects both water vapor partial pressure P_{H_2O} and temperature T as derived by the band integrated intensity technique and the infrared band ratio technique. The band ratio technique is readily seen to be the worse of the two, returning temperatures moderately in error and water vapor partial pressures grossly in error for rather small values of m (few percent). Based on this analysis, we attribute the observed differences in P_{H_2O} and T returned by these alternative techniques to the effects of inhomogeneous combustion. Also, in general, pressures, temperatures, and combustion efficiencies derived by the band integrated intensity technique can be regarded as upper bounds on the true mass averaged parameters.

A much milder perturbation to derived temperatures and water vapor partial pressures is caused by the slight expansion of the scramjet exhaust between the exit

plane and the point of observation 6 cm downstream. Depending upon test conditions, between 10–30 percent of the exhaust gas has undergone some degree of expansion at this point, with an approximate 10 percent drop in temperature. Assuming the larger 30 percent mass fraction limit for this expanded region, observed IR flux drops by 10 percent and deduced gas temperature by 3 percent. The effect of expansion upon derived water partial pressure is easier to describe since the actual water vapor distribution $P_{H_2O}(l)$ along the line of sight is simply related to the value obtained neglecting expansion by

$$P_{H_2O}l_0 = \int_{-\infty}^{\infty} P_{H_2O}(l)dl \quad (27)$$

where l_0 is the exit plane width. Thus, total water vapor abundances (pressure-path length product) are insensitive to expansion and are affected only by the propagation of slight temperature errors in the data analysis (i.e., 3 percent).

**TABLE 4 SENSITIVITY ANALYSIS OF THE INFRARED BAND RATIO AND BAND INTEGRATED INTENSITY TECHNIQUES TO INHOMOGENEOUS TEMPERATURE DISTRIBUTIONS
(1250K True mass averaged temperature)**

Mass Fraction m at 2000 K (%)	Band Integrated Intensity Results		Band Ratio Technique Results	
	P/P _{true}	T (K)	P/P _{true}	T (K)
0	1.00	1250	1.00	1250
1	1.07	1308	0.61	1415
2	1.13	1355	0.48	1516
3	1.18	1396	0.41	1585
4	1.23	1432	0.37	1634
5	1.27	1464	0.34	1671
6	1.31	1494	0.33	1700
7	1.34	1521	0.31	1723
8	1.37	1546	0.30	1742
9	1.40	1570	0.29	1757
10	1.43	1592	0.29	1771

CONCLUSIONS

The feasibility of remote sensing IR gas diagnostic techniques for the NASA Langley scramjet has been successfully demonstrated with interferometer spectrometer measurements of the $2.7\text{ }\mu\text{m}$ H_2O infrared emission band. The scramjet facility is characterized by adequate IR signal levels and acceptably low levels of thermal wall emission, flow contaminants, and reflected engine hot parts emission. Time-averaged uniformity of the scramjet exhaust properties is good, but the detailed IR emission time history indicates nonsteady turbulent behavior of the exhaust. Temperatures and water vapor partial pressures of the exhaust were deduced from the spectral data using the infrared band ratio technique and the band integrated intensity technique. The latter technique was shown to be superior because of poorly behaved error propagation properties in the former. Combustion efficiencies were derived by combining derived exhaust gas parameters with the known operating conditions of the scramjet engine. Derived efficiencies exhibited a general trend of falling efficiencies (70–50 percent) with rising fuel equivalence ratio (0.4–1.0).

The interferometer IR measurements provide a useful data base for the conceptual design and optimization of alternative optical gas diagnostic instrumentation. The experimental results clearly indicate requirements for good signal averaging capabilities and well behaved error propagation. Measurements of hot band optical properties ($h\nu \gg k_bT$), for example, are apt to give misleading results. Of the standard IR sensing techniques, emission-absorption (Ref. 9) appears to satisfy both these criteria with the added advantage of relative simplicity.

APPENDIX

PROCEDURE FOR UP-DATING RESULTS

Scramjet exhaust properties tabulated in Table 3 of this report are predicated upon certain assumptions and relations that are subject to change and improvement with time. It is therefore of value to outline a procedure for generating new and improved estimates of exhaust gas temperature, water vapor content, and efficiency. Errors in static pressure and in fuel equivalence ratio ϕ_1 affect only combustion efficiency η as defined in Eq. (13), so that the effects of spillage or error in the air flow capture ratio can be correctly evaluated using temperature and H_2O values from Table 3. These latter two parameters are only modified if the form of the theoretical temperature-water vapor relation (Eq. (21)) is modified. New temperature and water vapor values are deduced from the modified theoretical law through the use of the tabulation listed here. This tabulation lists for each run the locus of points in the $T - P_{H_2O}$ plane consistent with the experimentally observed IR band integrated intensities \bar{I} (see Eq. (5)). This relation, together with the theoretical prediction, form two equations in the two unknowns T and P_{H_2O} that may be solved either graphically or numerically. Water vapor values listed are in units of N/m (i. e., pressure-path length product) and can be converted to pressure units using the 16.2 cm width of the engine exit plane.

Run 165		Run 164	
$\phi_1 = .41$		$\phi_1 = .49$	
<u>H₂O, N/m</u>	<u>T, K</u>	<u>H₂O, N/m</u>	<u>T, K</u>
10.2	1800	29.1	1800
10.6	1775	30.4	1775
11.1	1750	31.8	1750
11.6	1725	33.3	1725
12.2	1700	34.8	1700
12.8	1675	36.5	1675
13.3	1650	38.4	1650
14.0	1625	40.3	1625
14.8	1600	42.5	1600
15.6	1575	44.7	1575
16.5	1550	47.3	1550
17.5	1525	50.0	1525
18.54	1500	53.1	1500
19.6	1475	56.3	1475
20.9	1450	59.9	1450
22.3	1425	63.9	1425
23.8	1400	68.2	1400
25.5	1375	73.1	1375
27.4	1350	78.4	1350
29.4	1325	84.4	1325
31.8	1300	91.1	1300
34.4	1275	98.5	1275
37.3	1250	106.9	1250
40.6	1225	116.4	1225
44.4	1200	127.2	1200
48.8	1175	139.6	1175
53.7	1150	153.7	1150
59.3	1125	169.9	1125
65.8	1100	188.6	1100
73.5	1075	210.5	1075
82.4	1050	236.1	1050
92.9	1025	266.3	1025
105.5	1000	302.1	1000
120.4	975	344.9	975
138.3	950	396.5	950
160.2	925	459.2	925
187.1	900	536.1	900
220.3	875	631.4	875
262.0	850	750.8	850
314.8	825	902.0	825
382.6	800	1096.3	800

Run 166	$\phi_1 = .85$	Run 164	$\phi_1 = .98$
H ₂ O, N/m	T, K	H ₂ O, N/m	T, K
66.3	1800	74.7	1800
69.2	1775	77.9	1775
72.3	1750	81.4	1750
75.6	1725	85.2	1725
79.2	1700	89.2	1700
83.0	1675	93.5	1675
87.1	1650	98.1	1650
91.6	1625	103.1	1625
96.4	1600	108.6	1600
101.7	1575	114.5	1575
107.4	1550	121.0	1550
113.7	1525	127.9	1525
120.5	1500	135.7	1500
127.9	1475	144.0	1475
136.1	1450	153.2	1450
145.1	1425	163.3	1425
155.0	1400	174.5	1400
166.0	1375	186.9	1375
178.2	1350	200.5	1350
191.7	1325	215.8	1325
206.9	1300	232.9	1300
233.9	1275	252.0	1275
243.0	1250	273.6	1250
264.7	1225	297.9	1225
289.2	1200	325.5	1200
317.2	1175	357.0	1175
349.1	1150	393.1	1150
386.0	1125	434.6	1125
428.7	1100	482.7	1100
478.4	1075	538.6	1075
536.5	1050	604.0	1050
605.1	1025	681.2	1025
686.4	1000	772.7	1000
783.6	975	882.2	975
900.9	950	1014.2	950
1043.3	925	1174.5	925
1218.0	900	1371.2	900
1434.6	875	1615.0	875
1705.9	850	1920.3	850
2049.6	825	2307.3	825
2490.9	800	2804.1	800

REFERENCES

1. Waltrup, Paul J, Anderson, Griffin Y, and Stull, Frank D., "Supersonic Combustion Ramjet (Scramjet) Engine Development in the United States," 3rd Int. Symp. Airbreathing Engines, Munich, Germany, March 1976.
2. Guy, R. W. and Mackley, E. A., "Initial Wind Tunnel Tests at Mach 4 and 7 of a Hydrogen Burning Airframe-Integrated Scramjet," 4th Int. Symp. Air Breathing Engines, Lake Buena Vista, Fla., April 1979.
3. Reed, R. A., "Fourier Transform Infrared Spectroscopy, Demonstration of Capabilities in the Laboratory and the Field," Grumman Research Department Memorandum RM-648, January 1978.
4. Taylor, L. S., "Infrared Noise Caused by Turbulent Flows," Applied Optics Vol. 17, p. 3911, 1978.
5. Martinsen, R. A. and Fishburne, E. S., "A Fine Spectral Resolution (FSR) Program for the Calculation of Infrared Radiation Emitted by Exhaust Plumes," Grumman Research Department Memorandum RM-575, July 1973.
6. Young, S. J., "Evaluation of Non-Isothermal Band Models for H_2O ," J. Quant. Spectros. Rad. Transfer, Vol. 18, p. 29, 1978.
7. Ferrisco, C. C., Ludwig, C. B., and Boynton, F. P., "A Band Ratio Technique for Determining Temperatures and Concentrations of Hot Combustion Gases from Infrared Emission Spectra," Proc. 10th Intl. Symp. Combustion, p. 161, 1965.
8. Herzberg, G., Molecular Spectra and Molecular Structure, "Vol. I: Diatomic Molecules," Sec. III.2, D. Van Nostrand, N. Y., 1950.
9. Brewer, L. E. and Limbaugh, C. C., "Infrared Band Model Technique for Combustion Diagnostics," Applied Optics Vol. II, p. 1200, 1972.

1. Report No. NASA CR- 3242		2. Government Accession No.		3. Recipient's Catalog No.	
4. Title and Subtitle INFRARED MEASUREMENTS OF A SCRAMJET EXHAUST				5. Report Date January 1980	
				6. Performing Organization Code	
7. Author(s) R. A. Reed and M. W. Slack				8. Performing Organization Report No.	
				10. Work Unit No. 505-05-43-01	
9. Performing Organization Name and Address Grumman Aerospace Corporation Bethpage, NY 11714				11. Contract or Grant No. NAS1-15395	
				13. Type of Report and Period Covered Contractor Report	
12. Sponsoring Agency Name and Address National Aeronautics and Space Administration Washington, D.C. 20546				14. Army Project No.	
15. Supplementary Notes Langley Technical Monitor: Marvin G. Torrence Final Report					
16. Abstract Diagnostic 2-5 μ m infrared spectra of a hydrogen burning scramjet exhaust were measured with an interferometer spectrometer. Exhaust gas temperatures and water vapor partial pressures were determined from the observed intensity and spectral profile of the H ₂ O 2.7 μ m infrared emission band. Overall engine combustion efficiencies were derived by combining these measurements with the known engine operating conditions. Efficiencies fall (70-50 percent) as fuel equivalence ratios rise (0.4-1.0). Data analysis techniques and sensitivity studies are also presented.					
17. Key Words (Suggested by Author(s)) Airbreathing Propulsion Scramjet			18. Distribution Statement Unclassified - Unlimited Subject Category 07		
19. Security Classif. (of this report) Unclassified	20. Security Classif. (of this page) Unclassified	21. No. of Pages 24	22. Price* \$4.00		